



**Special Sensor Microwave Imager and Sounder (SSMIS)
Antenna Brightness Temperature Data Record (TDR)
Calibration and Validation
User Manual**

**Center for Satellite Applications and Research
NOAA/NESDIS**

March, 2007

Approval Page



**Center of Satellite Applications and Research
National Environmental Satellite, Data, and Information Service
National Oceanic and Atmospheric Administration**

SSMIS TDR Cal/Val User Manual

Dr. Fuzhong Weng, Chief
Sensor Physics Branch
Satellite Meteorology and Climate Division
NOAA/NESDIS/Center for Satellite Applications and Research

Contributors from:

Banghua Yan (Lead), QSS/JCSDA
Ninghai Sun, IMSG/JCSDA
Masahiro Kazumori, EMC/JCSDA, visiting scientist from JMA
Nancy Baker, NRL
Steve Swadley, NRL
William Bell, Metoffice, UK
Yong Han, STAR/JCSDA
Mark Liu, QSS/JCSDA

Distribution to:

Ralph Ferrao, STAR	Tom Schott, OSD
Limin Zhao, OSDPD	Jim Silva, OSD
Hangjun Ding, OSDPD	Jean-Luc, Moncet, AER
A.K. Sharma, OSDPD	Don Bucher, Aerospace
Paul Chang, STAR	Yiping Wang, FNMOC
Sid Boukabara, IMSG	Jeff Tesmar, FNMOC
Bruce Thomas, AFWA	Gene Poe, NRL
Frank Wentz, RSS	Gail Jackson, GSFC
Stephen Lord, EMC	John Derber, EMC
Simon Chang, NRL	Joe Turk, NRL

Acknowledgement: This research is supported through the funding of Joint Center for Satellite Data Assimilation (JCSDA) Science Development and Implementation (JSDI) Task

Table of Contents

Section	Page
1 STATEMENT OF PROBLEM.....	3
2.1 SSMIS Lower Atmospheric Sounding Channels	6
2.1.1 Removal of warm load anomalies	6
2.1.2 Reflector emission correction.....	7
2.1.3 Preliminary Assessment of Recalibrated SSMIS Data at LAS Channels	9
2.2 SSMIS Imager Channels	11
2.2.1 Intersensor Calibration Methodology.....	11
2.2.2 SCO Quality Control.....	12
2.2.3 Linear Mapping.....	12
2.2.4 Nonlinearity Analysis.....	13
2.3 SSMIS Upper Atmospheric Sounding Channels.....	14
3 SSMIS PRODUCT VALIDATION.....	17
4 IMPACTS OF F16 SSMIS RECALIBRATION.....	23
4.1 Performance of Recalibrated SSMIS Data	23
4.2 Impacts on NWP Analysis, Forecast and Climate Reanalysis.....	25
5 STRENGTH AND WEAKNESS	30
5.1 NESDIS Calibration Strengths	30
5.2 NESDIS Calibration Weakness.....	31
References.....	32

1 STATEMENT OF PROBLEM

The Special Sensor Microwave Imager Sounder (SSMIS) was successfully launched aboard the Defense Meteorology Satellite Program (DMSP) F-16 satellite on October 18, 2003. It combines the channel frequencies of three previous DMSP instruments (SSMT, SSMT/2, SSM/I) into a single sensor, and measures the thermally emitted radiation from the Earth at 24 channels from 19 to 183 GHz. For reference purposes, 24 channels are grouped into four sub-types corresponding to the lower atmospheric sounding (LAS) channels (e.g., channels 1-7), the upper atmospheric sounding (UAS) channels (e.g., channels 19-24), the imaging (IMA) channels (i.e., channels 8-11, and 17-18) and the environmental (ENV) channels (e.g., channels 12-16), (Poe et al. 2001). Their specifications are given in Table 1, the scan geometry and weighting functions are displayed in Figure 1a and 1b. As such, the SSMIS offers improved atmospheric temperature soundings, water vapor soundings and surface observations, in comparison to those of the previous DMSP instruments.

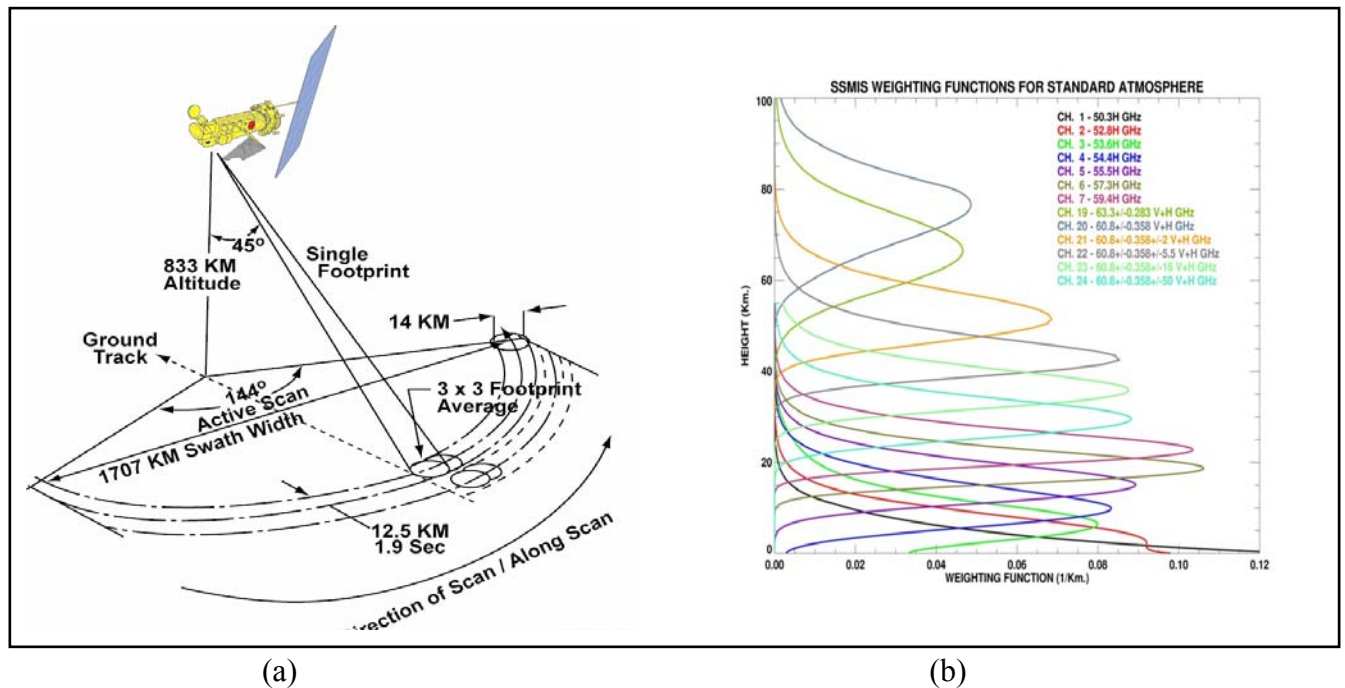


Figure 1 (a) SSMIS scan geometry. (b) SSMIS weighting functions for a standard atmosphere, (Poe et al., 2001).

TABLE 1 Channel characteristics of F16 SSMIS sensor, (Poe et al., 2001)

Channel	Center Freq.(GHz)	3-db Width (MHz)	Freq. Stab.(MHz)	Pol.	NEDT (K)	Sampling Interval(km)
1	50.3	380	10	V	0.34	37.5
2	52.8	389	10	V	0.32	37.5
3	53.596	380	10	V	0.33	37.5
4	54.4	383	10	V	0.33	37.5
5	55.5	391	10	V	0.34	37.5
6	57.29	330	10	RCP	0.41	37.5
7	59.4	239	10	RCP	0.40	37.5
8	150	1642(2)	200	H	0.89	12.5
9	183.31+/-6.6	1526(2)	200	H	0.97	12.5
10	183.31+/-3	1019(2)	200	H	0.67	12.5
11	183.31+/-1	513(2)	200	H	0.81	12.5
12	19.35	355	75	H	0.33	25
13	19.35	357	75	V	0.31	25
14	22.235	401	75	V	0.43	25
15	37	1616	75	H	0.25	25
16	37	1545	75	V	0.20	25
17	91.655	1418(2)	100	V	0.33	12.5
18	91.655	1411(2)	100	H	0.32	12.5
19	63.283248+/-0.285271	1.35(2)	0.08	RCP	2.7	75
20	60.792668+/-0.357892	1.35(2)	0.08	RCP	2.7	75
21	60.792668+/-0.357892+/-0.002	1.3(4)	0.08	RCP	1.9	75
22	60.792668+/-0.357892+/-0.0055	2.6(4)	0.12	RCP	1.3	75
23	60.792668+/-0.357892+/-0.016	7.35(4)	0.34	RCP	0.8	75
24	60.792668+/-0.357892+/-0.050	26.5(4)	0.84	RCP	0.9	37.5
Notes	(1) Sampling refers to along scan direction based on 833km spacecraft altitude. (2) NEDT for instrument temperature 0C and calibration target 260K with integration times of 8.4 msec for Channels 12-16; 12.6 msec for Channels 1-7, 24; and 25.2 msec for Channels 19-23 and 4.2 msec for Channels 8-11, 17-18. (3) Number of sub-bands is indicated by (n) next to individual 3-db width (4) RCP denotes right-hand circular polarization.					

However, the F16 SSMIS displays obvious anomalies in radiances, which have been detected from the difference between global Radiative Transfer Modelling (RTM) simulated and observed brightness temperatures (Swadley et al., 2005; Weng et al., 2005; Bell et al., 2005). One powerful tool that has received considerable attention in NOAA satellite cal/val research is the comparison of radiances computed from Numerical Weather Prediction (NWP) model analyses with observed radiances. The major NWP centres make these comparisons on a daily basis for the instrument data

that are assimilated in the models. Although the NWP model and its associated radiative transfer system have their own biases, the model calculations can be used reference beyond its own bias. Model versus observation comparisons can be used to determine the bias of one instrument relative to another or the stability of an instrument over time. Shown in Figure 2 is the difference between simulated and observed brightness temperatures for F-16 SSMIS 54.4 GHz. The anomaly in SSMIS radiances is observed and its pattern depends strongly on geolocation and season (Yan and Weng, 2007a).

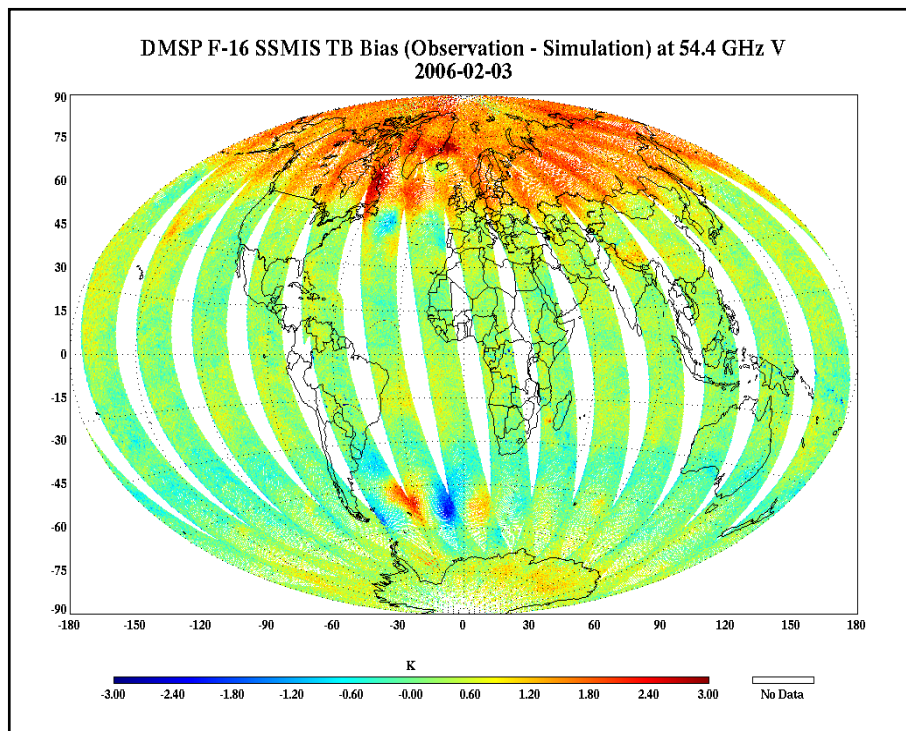


Figure 2 The difference between simulated and observed brightness temperatures for Defense Meteorological Satellite Program (DMSP) F-16 Special Sensor Microwave Imager and Sounder (SSMIS) 54.4 GHz. The largest biases as colored red result from the contamination of satellite antenna emission. Correcting unintended instrument contamination is now part of the cal/val process to provide accurate data for use in computerized weather forecast models

To remove those anomalies, three independent preprocessors for SSMIS radiances are currently available, at various stages of development (Swadley et al., 2007; Bell et al., 2007; Yan and Weng, 2007a). It is probably fair to say that none of these preprocessors would be described by their

authors as *definitive* but represent their best efforts to date to correct the instrumental biases evident in F-16 SSMIS data. There is a desire in the wider assimilation community that we form a strategy which will result in the establishment of a single datastream of corrected SSMIS radiances which will incorporate the best corrections we have to date. The purpose of the comparison at NRL will be to establish, by consensus, what are the best corrections for SSMIS radiances. In this manual, the NOAA preprocessor for SSMIS radiances developed by Yan and Weng (2007a) is introduced.

2 NOAA SSMIS TDR RECALIBRATION

NESDIS anomaly mitigation preprocessor was designed to work in conjunction with the operational SSMIS Ground Processing Software (GPS). The intent of the preprocessor was to produce a new TDR file, with minimal file format and structure changes to be used for subsequent radiance assimilation and/or distribution in BUFR for the larger community of SSMIS TDR users, i.e., the NWP radiance assimilation community. NESDIS recalibration processes SSMIS TDR differently according to lower, upper and imager channels.

2.1 SSMIS Lower Atmospheric Sounding Channels

2.1.1 Removal of warm load anomalies

For an orbit of observations, the solar intrusion results in fluctuations of observed warm counts (C_w^{Obs}), as shown in Figure 3. In the domain of frequency, those fluctuations represent some higher frequency components superimposed on C_w^{Obs} over the corresponding areas, in comparison to the slow frequency component of one orbit of observations with a period of 102 minutes. So, the correction of warm count anomaly is made by applying FFT analysis to an orbit of warm target counts (Yan and Weng, 2007a). There, we can filter out major high- frequency components in C_w^{Obs} related to direct solar and stray light contamination and obtain a relatively smooth distribution for C_w^{Obs} .

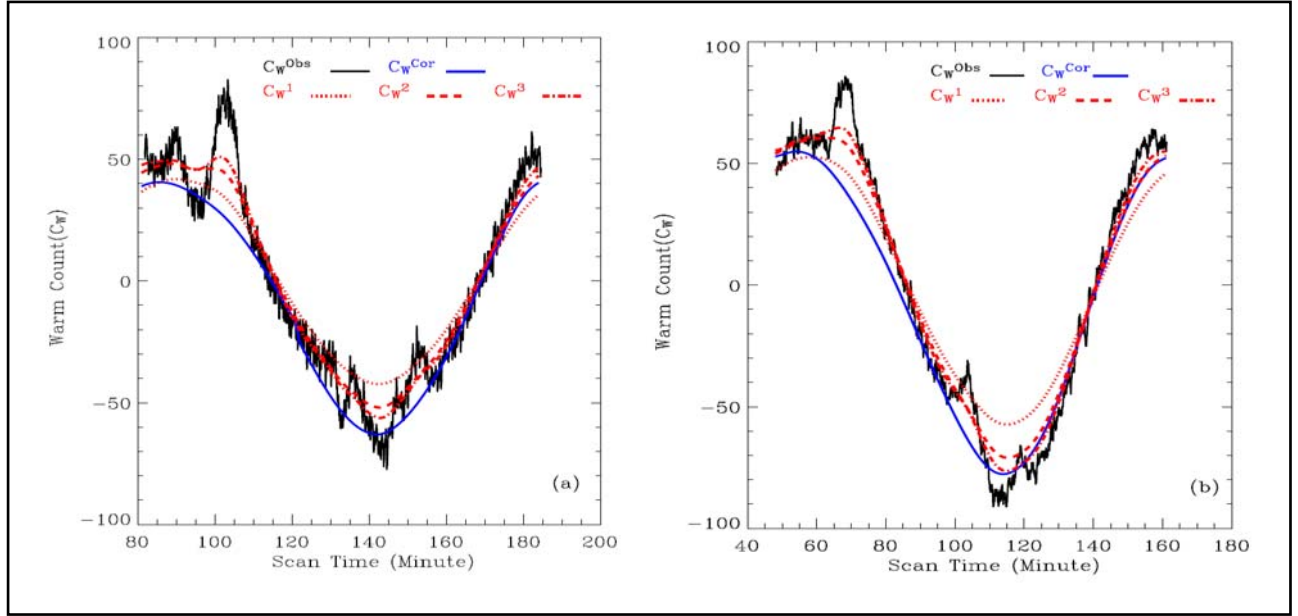


Figure 3 Time series of C_W^{Obs} , C_W^1 , C_W^2 , C_W^3 , C_W^{Cor} at 54.4 GHz during one orbit of observations, where C_W^{Obs} is the observed radiometric counts of the blackbody target, C_W^m the first m-th harmonic components in C_W^{Obs} using FFT harmonic analysis, C_W^{Cor} the anomaly-reduced warm counts, (Yan and Weng, 2007a). (a) March 20, 2005. (b) June 9, 2005.

As shown in Fig. 3, the newly calibrated counts (C_W^{Cor}) capture the basic feature of observed warm counts in the absence of solar intrusion. Then, regions where ΔC_W ($C_W^{Obs} - C_W^{Cor}$) exceeds a certain threshold are reliably identified and the calibration correction is required using the following equation.

$$\Delta T_A^{CAL} = - \left[\frac{T_A - T_C}{C_W - C_C} \right] \Delta C_W - \left[\frac{T_W - T_A}{C_W - C_C} \right] \Delta C_C + \left[\frac{C_S - C_C}{C_W - C_C} \right] \Delta T_W, \quad (1)$$

where C_S , C_C , and C_W denote the counts of earth scene, cold space, and warm target, respectively; T_C is the deep space cosmic background temperature, and T_W is the brightness temperature of the warm target, which is determined by the physical temperature (the warm target emissivity is considered close to unity) measured using Platinum Resistance Thermistors (PRT's). Note that the superscription 'Obs' is omitted from C_W and other observed parameters.

2.1.2 Reflector emission correction

The SSMIS main reflector is paraboloidal so that the incoming radiation is focused on the feedhorns which transfer the free-space wave to a guided wave. As the main reflector views earth, it collects the incoming radiation over an angular distribution defined by the antenna gain pattern, where the coming radiance is convolved with the gain function of the reflector and is further focused on a specific feedhorn to produce the antenna temperature of the earth scene. So, the antenna temperature is given by

$$T'_A = (1 - \varepsilon_R)T_A + \varepsilon_R T_R \quad (2)$$

with

$$T_A = \frac{\int_0^{2\pi} \int_0^{2\pi} T_B^{Earth}(\theta, \varphi) G(\theta, \varphi) \sin \theta \, d\theta \, d\varphi}{\int_0^{2\pi} \int_0^{2\pi} G(\theta, \varphi) \sin \theta \, d\theta \, d\varphi}, \quad (3)$$

$$T_R = \frac{\int_0^{2\pi} \int_0^{2\pi} T_R^{Phy}(\theta, \varphi) G(\theta, \varphi) \sin \theta \, d\theta \, d\varphi}{\int_0^{2\pi} \int_0^{2\pi} G(\theta, \varphi) \sin \theta \, d\theta \, d\varphi}. \quad (4)$$

where, $G(\theta, \varphi)$ is the gain function of the reflector, with ε_R being the reflector emissivity. Equation (2) contains the antenna temperature of the earth scene, T_A , whose brightness temperature is T_B^{Earth} , T_R , whose physical temperature is T_R^{Phy} . Note that the reflector temperature varies with polarization and frequency.

For LAS channels, the reflector temperatures are computed from the arm temperature with a suitable adjust ($\Delta T_{R,ich}$), i.e.,

$$T_{R,ich}(\varphi) = T_{ARM}(\varphi) + \Delta T_{R,ich}(\varphi), \quad (5)$$

$$\Delta T_{R,ich}(\varphi) = a_{0i} + \sum_{j=1}^6 a_{ji} \varphi^j, \quad (6)$$

where the subscript ‘ich’ represents the i th channel among LAS channels. ΔT_R is determined by using a group of polynomial expressions in terms of latitude. The fitting coefficients of polynomial expressions are derived from the training data sets of T_R (and T_{ARM}), and this T_R is generated by solving (2) with the RTM simulations at several oxygen sounding channels between 54.4 and 59.4

GHz, (Yan and Weng, 2007a). At other LAS channels except for frequencies from to 59.4 GHz, the reflector temperature is approximated by that at 54.4 GHz (Yan and Weng, 2007a). As an example, Figure 4 shows the reflector arm temperature, the retrieved and fitted reflector temperatures at 54.4 GHz, on March 20, 2006.

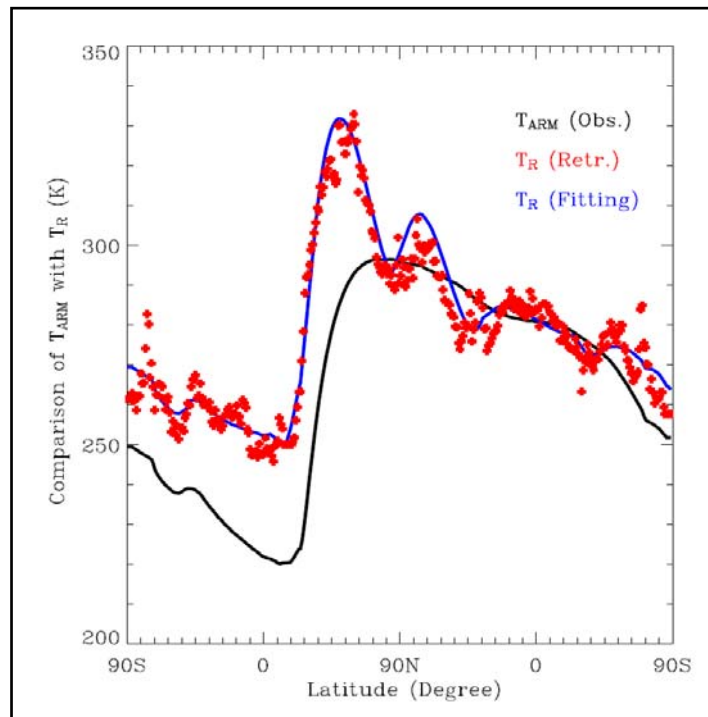


Figure 4 Comparisons of the observed arm temperature, the retrieved and fitted reflector temperatures at 54.4 GHz during one orbit of observations on March 20, 2005, (Yan and Weng, 2007a).

2.1.3 Preliminary Assessment of Recalibrated SSMIS Data at LAS Channels

Examination of the performance of recalibrated SSMIS data (CTDR) is made first from their comparisons with the radiative transfer model simulations and with AMSU observations. Figure 5 displays the difference between CTDR and simulated brightness temperatures (DTB) for F-16 SSMIS 54.4 GHz. Compared to SSMIS TDR data (Fig. 2), the brightness temperature anomalies are significantly reduced in CTDR data, where absolute biases are typically smaller than 0.5 K over most of the global areas and standard deviations are usually smaller than 0.3. Figure 6 displays inter-comparison of SSMIS and N16 AMSU-A in brightness temperatures at 53.6, 54.4, 55.5 and 57.3 GHz. It is recognized that the original SSMIS brightness temperatures are larger than these from NOAA-16 AMSU by around 2 K, which is consistent with the previous analyses. The SSMIS

brightness temperatures after the recalibration are in agreement with AMSU measurements. The mean differences in brightness temperatures between calibrated SSMIS and NOAA-16 AMSU measurements are smaller than 0.5 K at these three frequencies.

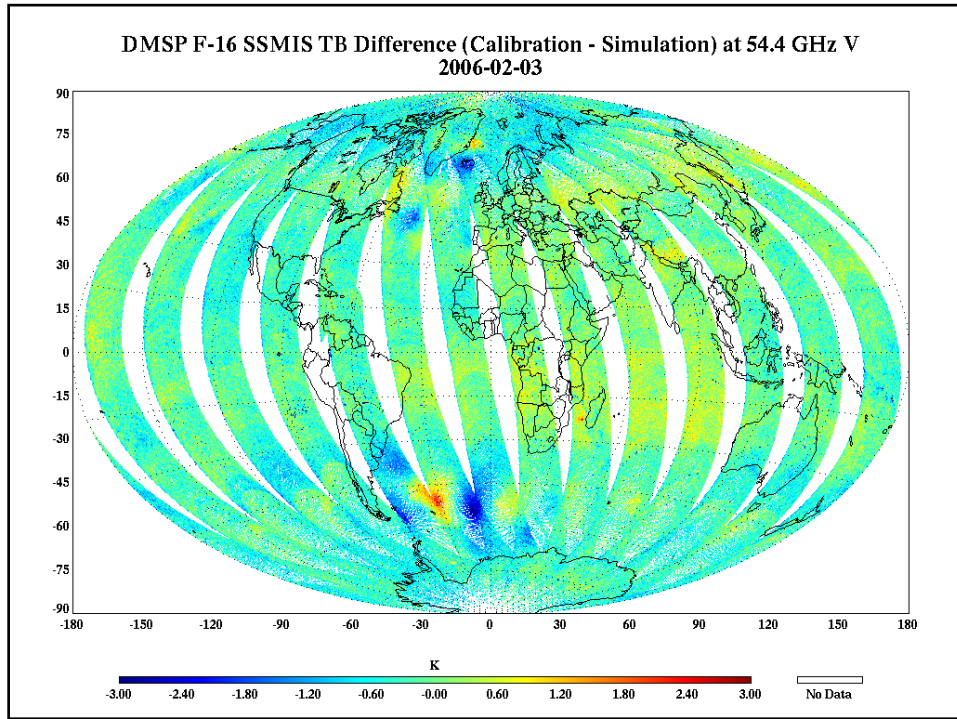
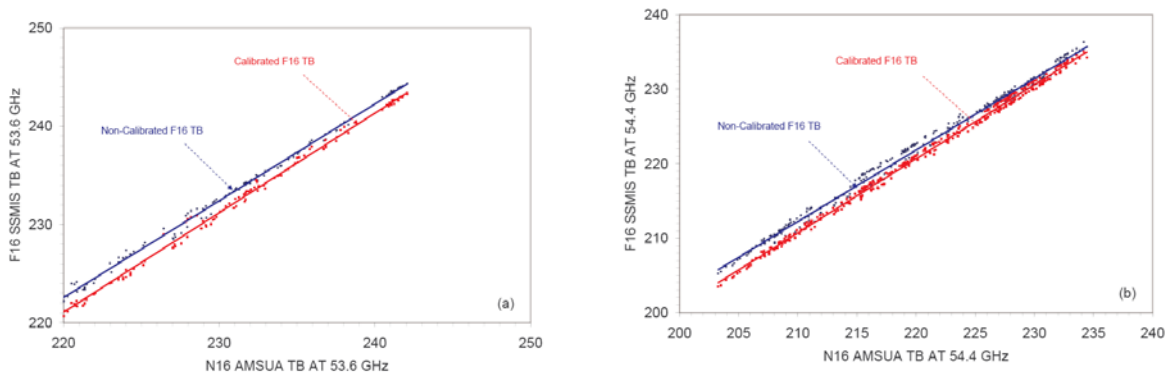


Figure 5 The difference between recalibrated SSMIS observed and simulated brightness temperatures for DMSP F-16 SSMIS 54.4 GHz.



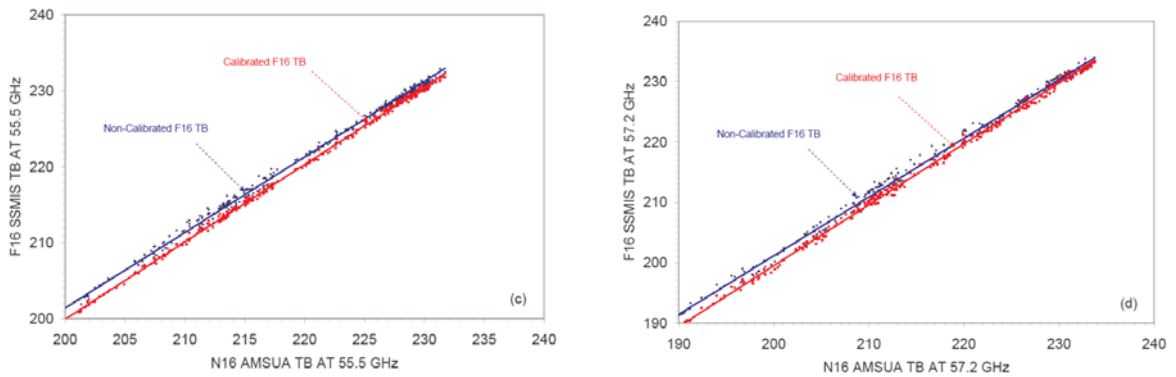


Figure 6 Inter-comparison of F16 SSMIS and N16 AMSU-A in brightness temperatures at 53.6, 54.4, 55.5 and 57.3 GHz (Yan and Weng, 2007a).

2.2 SSMIS Imager Channels

The SSMIS offers seven window channels (channels 12 – 18) to continue the capability of the DMSP Special Sensor Microwave Imager (SSM/I) in monitoring and retrieving atmospheric and surface parameters such as precipitation, sea ice, ocean surface wind speed, columnar integrated liquid water, land surface temperature and emissivity, and soil moisture (Ferraro et al., 1996; Weng et al., 1997; Ferraro, 1997; Yan and Weng, 2002; Yan et al., 2004). As analyzed above, F16 SSMIS brightness temperatures at sounding channels are severely contaminated by anomalous antenna emission and solar intrusions to its calibration targets. It is important to investigate the quality of SSMIS imaging channel calibration through intersensor calibration.

2.2.1 Intersensor Calibration Methodology

Recently, Cao et al. (2004) developed a method to predict the time and location of the Simultaneous Nadir Overpasses (SNO) for the purpose of intercalibration among the different NOAA satellites. Simultaneous observations between two satellites provide on-orbit monitoring of instrument performance through bias analysis and determination of instrument non-linearity. For two polar-orbiting satellites flying at different altitudes, a SNO event is found and a SNO data pair is generated when they cross each other, where they observe the same earth location at nadir at nearly the same time. A schematic viewing of the SNO event is shown in Figure 7, where two satellites (NOAA 16 and NOAA 17) approach other. For F15 and F16 satellites, the intercepting event happens once every 93.4 days on average. Here, we modify the algorithms for SSMIS and SSM/I intersensor calibration because both instruments are conically scanning and have more chances for

matching up in space and time. This is called Simultaneous Conical Overpass (SCO).

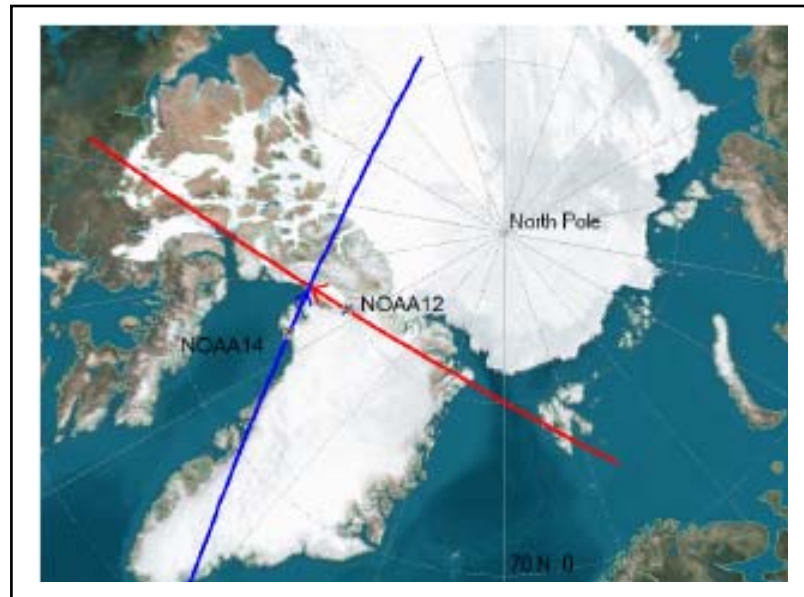


Figure 7 Schematic viewing the overpasses between two satellites.

2.2.2 SCO Quality Control

In our study, the SCO constraints on temporal and spatial windows are relaxed to have more matchup data, considering that the matching events mainly occur in high latitudes where surface and atmosphere are relatively stable. The distance window from two sensors is set to an Earth ground distance of 12.5 km and the time window is set to 60 seconds. In addition, a new data collocation technique developed by Ica vacci and Cao (2007) is used to reduce the effect of inhomogeneous surface properties on SCO observations at window channels. This is because window channels of microwave radiometers have relatively large fields of view and the satellite measurements near the two different surface boundaries (see ice and water) may display large contrasts in surface properties (Yan et al., 2004). By using this technique, SCO events over a location are rejected when their standard deviation is larger than 1 K.

2.2.3 Linear Mapping

In SSMIS calibration, we first tested direct linear mapping between SSMIS imaging channels and SSM/I using

$$T'_{A,ich} = \alpha_{ich} + \beta_{ich} T_{A,ich}, \quad (7)$$

where α_{ich} and β_{ich} denote the offset and slope correspondingly, and both of them are produced by using SCO observations between SSMIS and SSM/I; the subscription 'ich' is the SSMIS channel corresponding to each of the seven SSMI-like channels, i.e., $i = 11, 12, 13, 15, 14, 18, 17$. Table 2 displays the derived offset and slope values.

TABLE 2 Offset and slope values used in (7) for remapping F16 SSMIS antenna temperature at the seven SSMI-like channels to F15 SSMI antenna temperatures, (Yan and Weng, 2007b).

Frequency(GHz)	α	β
19.35 (V)	-2.03627	1.00623
19.35 (H)	0.00424	1.00027
22.235 (V)	-2.52875	0.99642
37 (V)	-3.86053	1.00550
37 (H)	0.80170	0.99139
91.65 (V)	-7.43913	1.03121
91.76 (H)	1.53650	0.99317

2.2.4 Nonlinearity Analysis

Antenna temperature (T_A) including non-linearity term is given as follows.

$$T_A = T_C + S(C_S - C_C) + \mu S^2(C_S - C_C)(C_S - C_W) = T_{AL} + \mu Z, \quad (8)$$

where

$$S = \frac{T_W - T_C}{C_W - C_C}, T_{AL} = T_C + S(C_S - C_C), Z = S^2(C_S - C_C)(C_S - C_W). \quad (9)$$

In SSMI/S calibration, the nonlinear parameter was not available from the pre-launch analysis. Those nonlinear parameters for F15 and F16 observations are derived from the SCO observations between F15 and F16 (Yan and Weng, 2007b), shown in Table 3.

Figures 8(a) - 8(e) show the time series of the linear and nonlinear calibrated SSMIS antenna temperature biases from 19.35 to 37 GHz, which are calculated from the linear calibration equation, i.e., ignoring the second term on the right side in (7), and the nonlinear calibration equation using

(7), respectively. One obvious feature is observed from the figures: the SSMIS antenna temperature biases are significantly reduced and the mean bias is usually smaller than 0.3, as the nonlinear calibration is applied into both F15 and F16 observations. Therefore, those preliminary results have demonstrated that the nonlinearity seems to be non-negligible in future SSM/I and SSMIS reprocessing.

Table 3 Nonlinear parameters (μ) in (1) at frequencies from 19.35 to 37 GHz for F15 and F16 observations, (Yan and Weng, 2007b)

Frequency(GHz)	Nonlinear Parameter (μ)	
	F15	F16
19.35 (V-POL)	-1.49910E-5	2.59475E-5
19.35 (H-POL)	-5.59600E-6	-9.49400E-6
22.235 (V-POL)	-6.61825E-5	7.73750E-5
37 (V-POL)	-6.20845E-5	7.23580E-5
37 (H-POL)	1.21750E-6	2.61885E-5

2.3 SSMIS Upper Atmospheric Sounding Channels

The activity is on-going to include correction for doppler shift, zeeman splitting.....

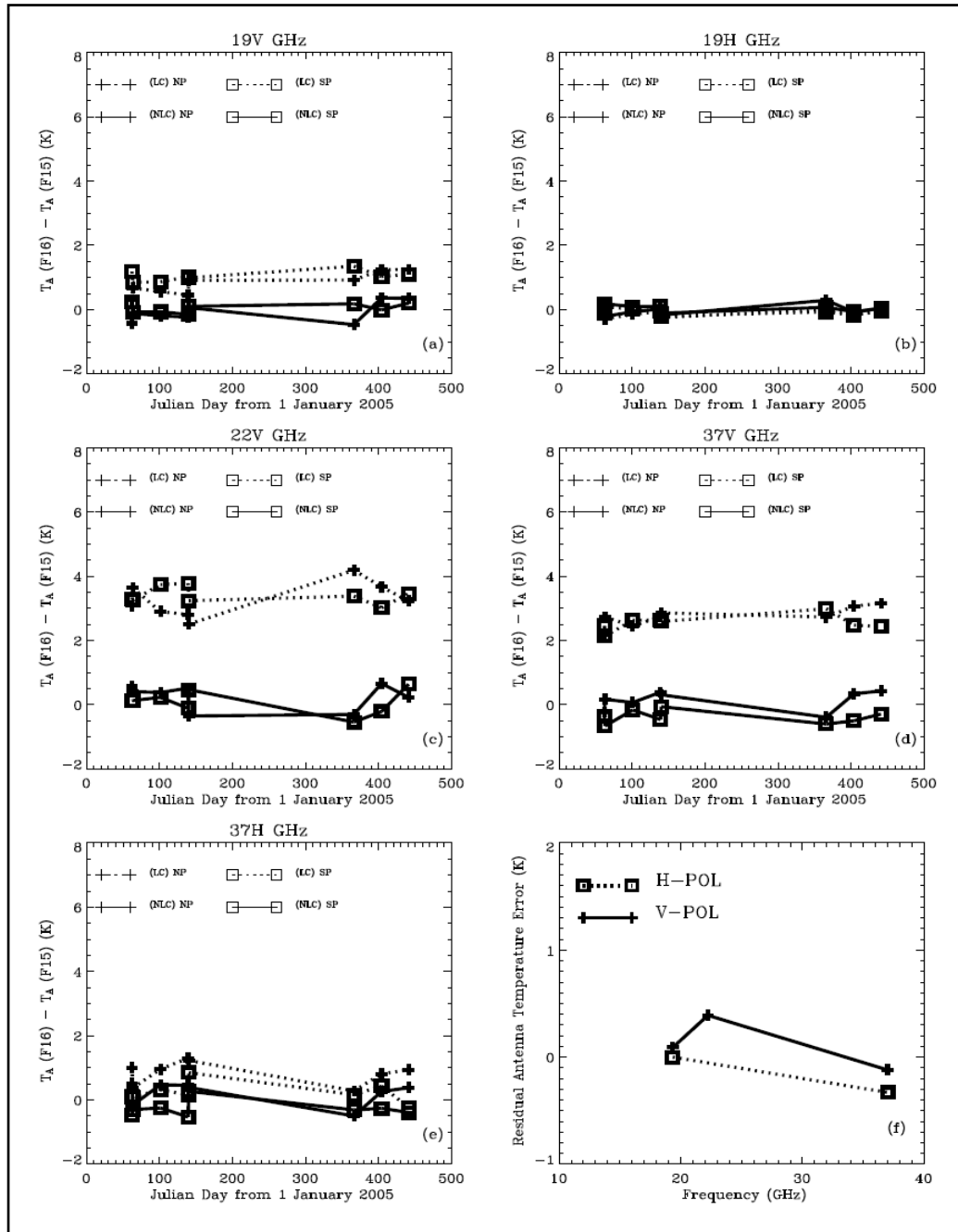


Figure 8 Time series of F16 antenna temperature biases at frequencies from 19.35 to 37 GHz, which are computed using linear and nonlinear calibration equations, respectively, (Yan and Weng, 2007b). In the figure, ‘LC’ denotes the linear calibration while ‘NLC’ the nonlinear calibration. (a) V-POL 19.35 GHz. (b) H-POL 19.35 GHz. (c) V-POL 22.235 GHz. (d) V-POL 37 GHz. (e) H-POL 37 GHz. (f) Residual antenna temperature difference at V/H-POL, after the nonlinear calibration is applied to both F15 and F16 observations.

2.4 Data Averaging and Collocation

The SSMIS over-samples in the along-track direction. These oversampled data can be used to reduce the SSMIS random noise. Two approaches are applied to the data averaging to reduce observation noise.

The first approach is to recalculate calibration target parameters, e.g., C_C , C_W , and T_W , from the simple average along certain scan lines corresponding to each observation location. For example, in our current NOAA preprocessor, the scene count (C_S) is first obtained from the antenna temperature through the linear calibration

$$C_S = C_C + \frac{(T_A - T_C)(C_W - C_C)}{(T_W - T_C)}. \quad (10)$$

Then, the antenna temperature is recalibrated by using the averaged calibration target parameters based upon 5 scan lines from an observed pixel, e.g., \bar{T}_W , \bar{C}_W , \bar{C}_C , as expressed as follows.

$$T'_A = T_C + \frac{(\bar{T}_W - T_C)(C_S - \bar{C}_C)}{\bar{C}_W - \bar{C}_C}, \bar{T}_W = \sum_{i=1}^5 T_{Wi}, \bar{C}_W = \sum_{i=1}^5 C_{Wi}, \bar{C}_C = \sum_{i=1}^5 C_{Ci}. \quad (11)$$

The second approach is to do data averaging over a certain domain by scan lines and pixels per scan line centered on each field of view according to their approximate weighting functions. We follow the methodology proposed by UK (Bell, 2006). The average antenna temperature field (T''_A) is computed from the antenna temperature field (T'_A) computed from (10) as follows.

$$T''_A = \sum_{l=1}^N w_i(p) T'_A(l + \delta_i(p), p'_i(p)) / \sum_{l=1}^N w_i(p), w_i(p) = \exp\left(-\frac{r_i^2}{2\sigma^2}\right), r_i = \text{distance}((l, p), (l + \delta^i(p), p'_i(p))), \quad (12)$$

where N is the domain size in terms of number of nearest neighbors used for averaging and has been chosen to 100. Except for UAS channels where $\sigma = 75.0$, $\sigma = 25.0$ for other channels.

As discussed in section 1, the four instrument subtypes for SSMIS have non-collocated footprints. Collocated data offers the benefits of simpler and more reliable cloud detection, and also enables various channels to be used to extrapolate temperatures above the model top. For these reasons the

SSMIS brightness temperatures are collocated in the pre-processor to the grid defined by the LAS observations. A similar approach to (12) is made in our preprocessor. This is done by using pre-computed interpolation coefficients. Firstly, each subtype brightness temperature data set is defined within a 2D array indexed by scan line (l) and scanposition (p). For each of the 60 LAS fields of view, the five nearest neighbors for each of the other scan types (UAS, IMA and ENV) are used to construct the antenna temperature at the LAS footprint location. For each channel, for each LAS footprint location, a weighted average of the four nearest neighbor radiances is computed.

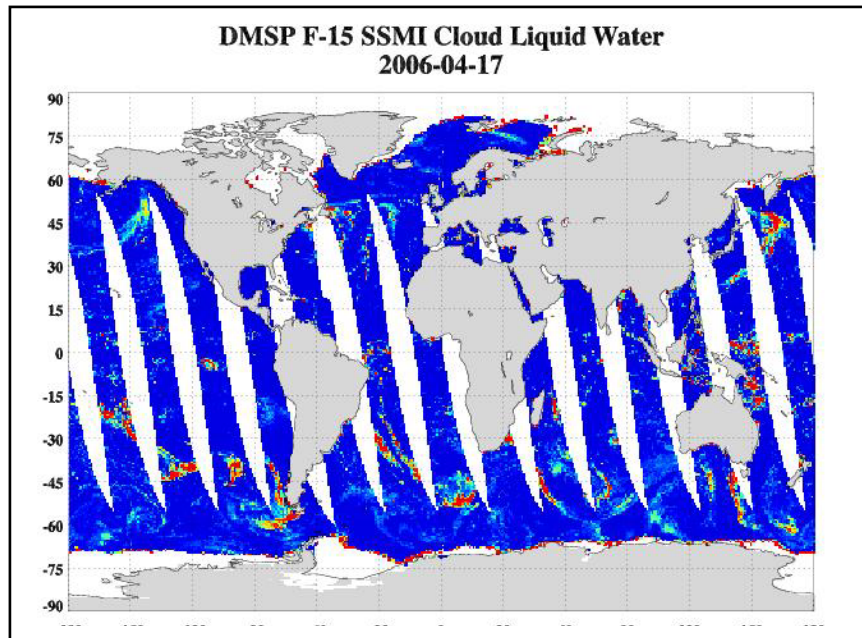
$$T_A^{LAS} = \sum_{i=1}^N w_i(p) T_A^{Non-LAS}(l + \delta_i(p), p'_i(p)). \quad (13)$$

3 SSMIS PRODUCT VALIDATION

The SSM/I measures the thermal radiation from the earth's surface and atmosphere at four frequencies between 19 and 85 GHz with vertical and horizontal polarizations and has provided the critical information on global hydrological parameters such as water vapor, cloud water and precipitation. Some of these products are also assimilated with the outputs from the numerical weather prediction models to improve global weather forecasts. Thus, as part of our validation activities, the products retrieved from SSMIS measurements are compared with those from SSM/I on board F-15 satellite, (Sun and Weng, 2007). As described above, our new calibration methodology is developed from the SSMI/S Temperature Data Records (TDR) which actually contains earth-located sets of antenna temperature. In the retrieval of parameters, not only antenna temperature but also brightness temperature will be used. The brightness temperature (Sensor Data Record or SDR) is obtained after Doppler correction, cross polarization and spill-over correction (or antenna pattern correction) on TDR data. Thus, two coefficients are used: 1) the coefficients in Table 2 which are applied to linearly map the SSMIS to F15 SSMI imaging channels at antenna temperature level (Calibrated TDR), and 2) the coefficients related to Doppler correction and cross polarization and spill-over correction (or antenna pattern correction) which are utilized to convert CTDR to SDR. The latter is provided by Navy Research Lab (NRL). Note that that this linear mapping also converts SSMI/S 91.655 GHz to 85.5 GHz.

The SSMI/S imaging products are generated using the algorithms developed previously by NESDIS and other research institutes. The products include rain rate, total precipitable water, cloud liquid water, surface skin temperature and land emissivity, as shown in Figures 9-13, (Sun and Weng,

2007). Overall, comparisons shows that after NESDIS algorithm is applied for correction on F16 SSMI/S contamination, the retrieval products are very consistent with those from the DMSP F-15.



(a)

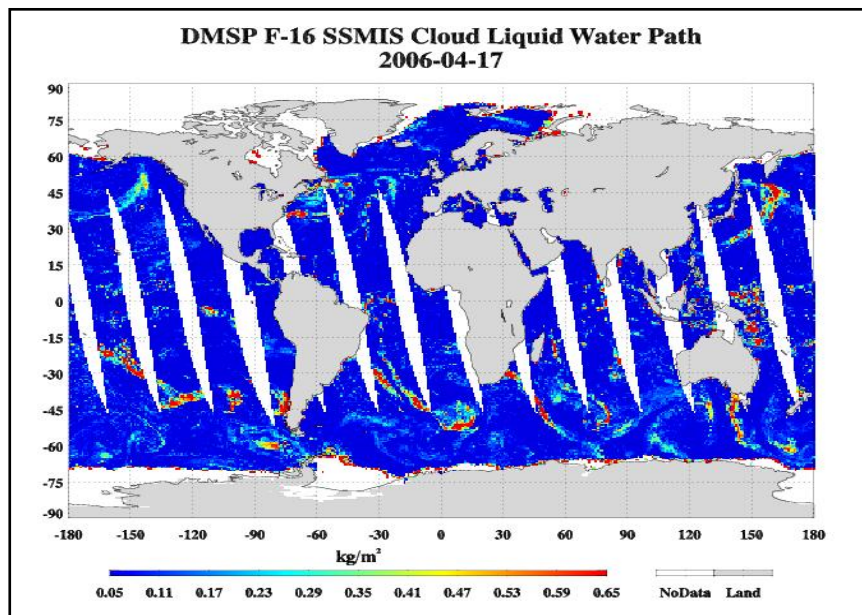
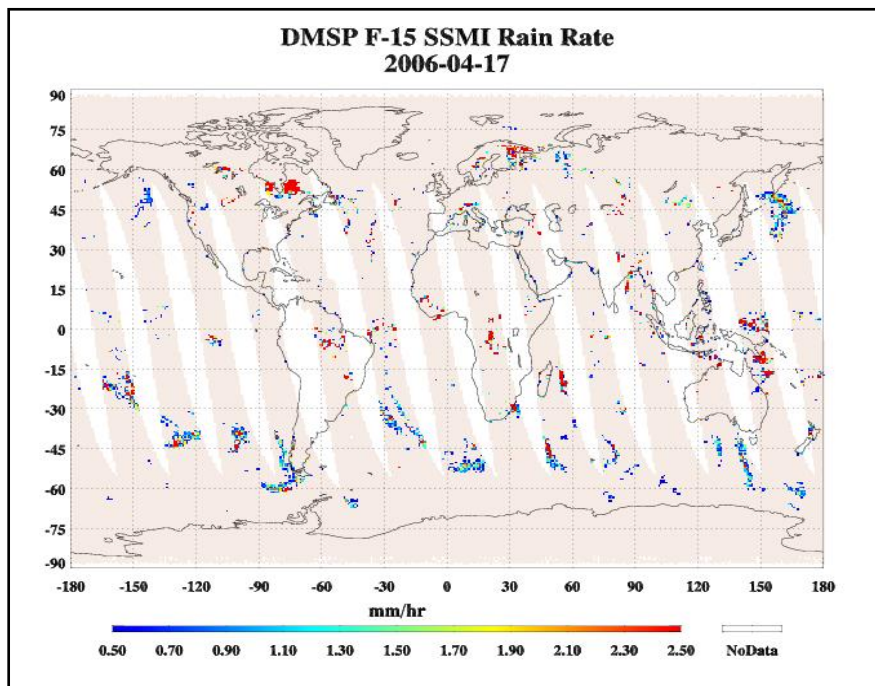
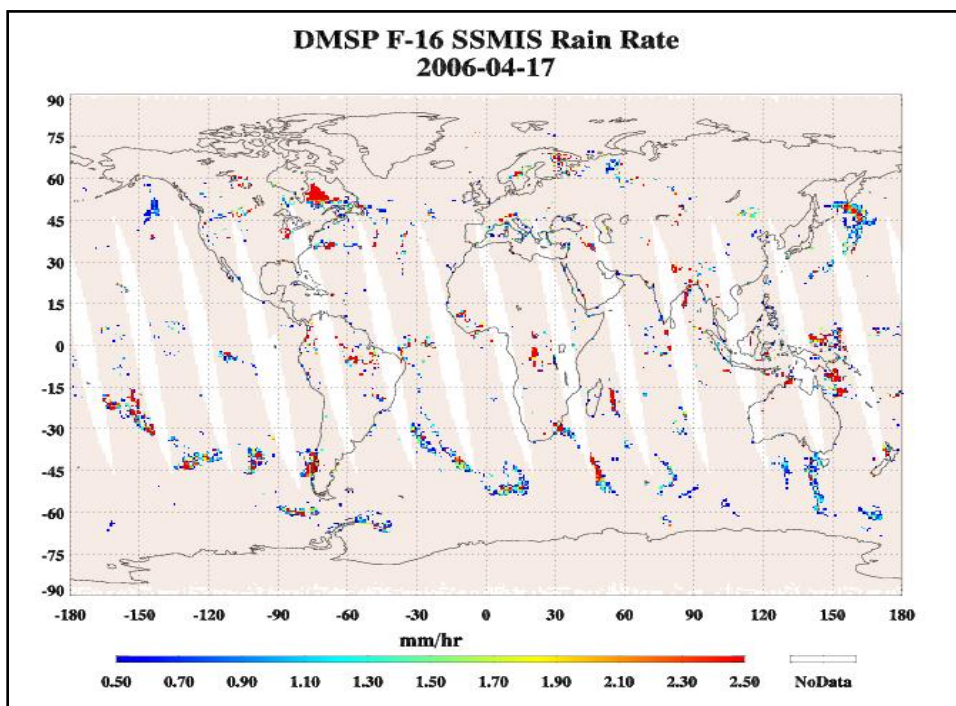


Figure 9 (a) Cloud Liquid Water Retrieved from DMSP F-15 SSM/I Imaging Channels on April 17, 2005.(b) Same as Figure-1 but from DMSP F-16 SSMI/S Imaging.

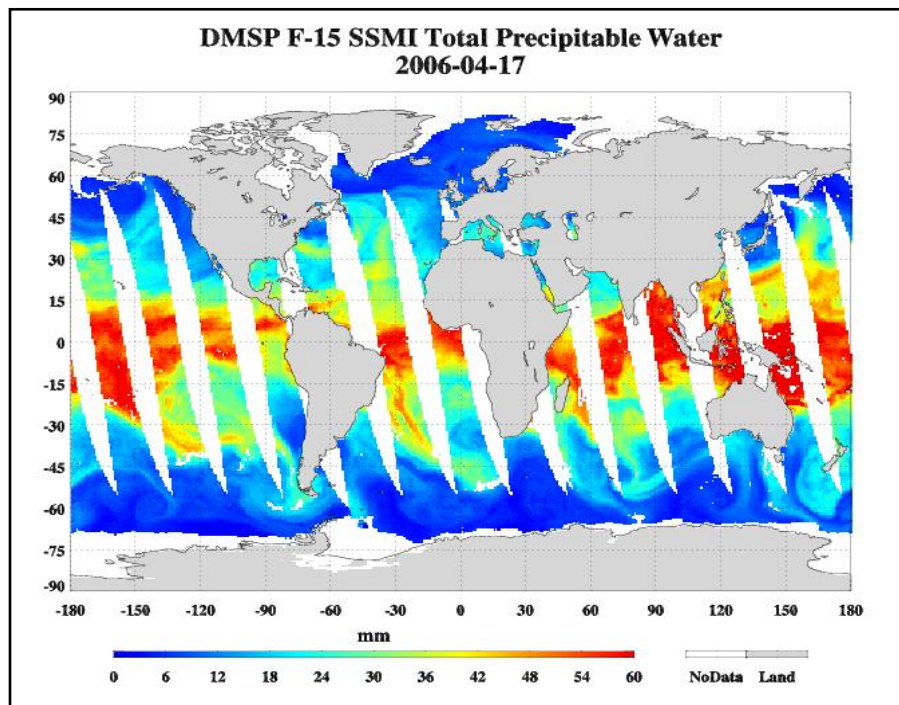


(a)

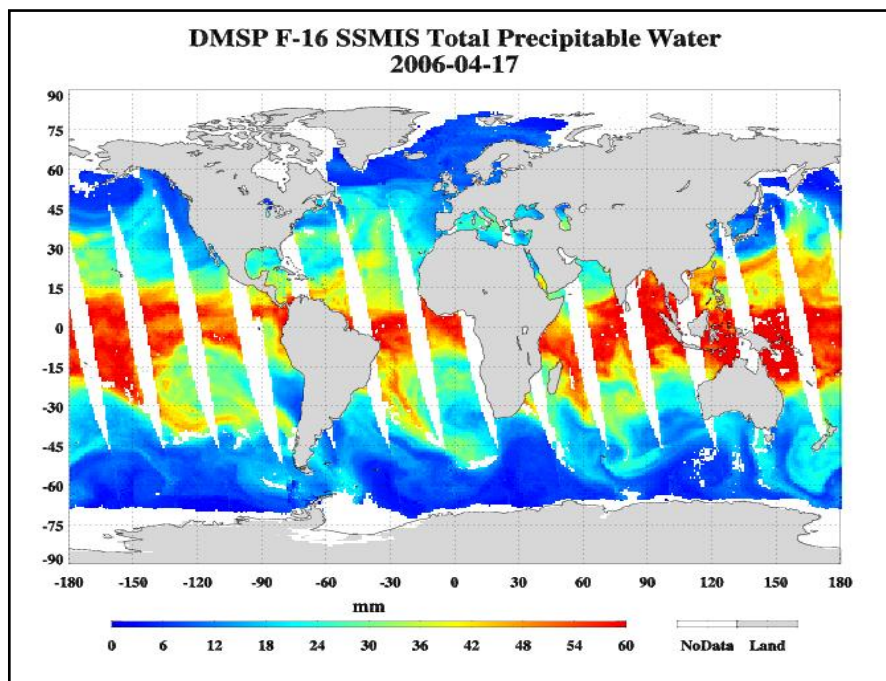


(b)

Figure 10 (a) Rain Rate Retrieved from DMSP F-15 SSM/I Imaging Channels on April 17, 2005. (b) Same as Figure-3 but from DMSP F-16 SSMI/S Imaging Channels

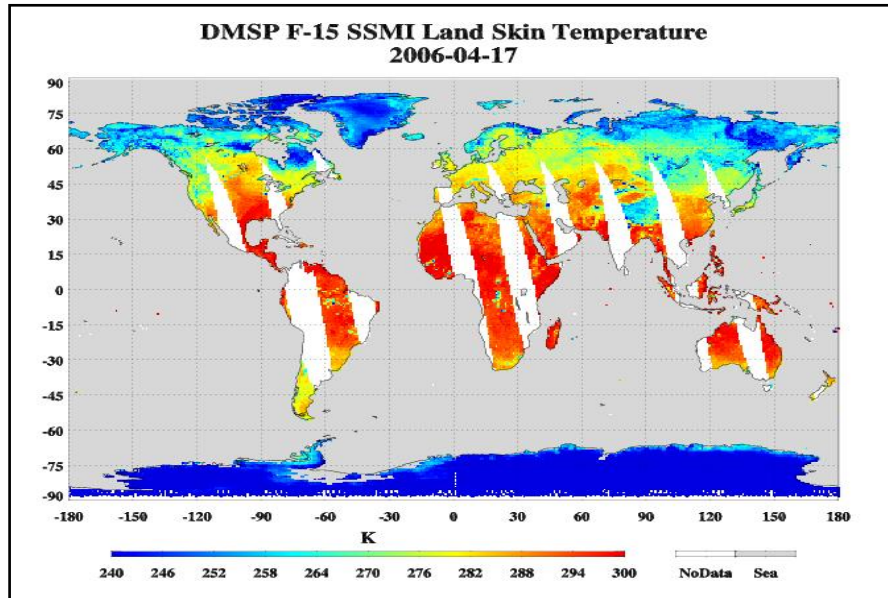


(a)

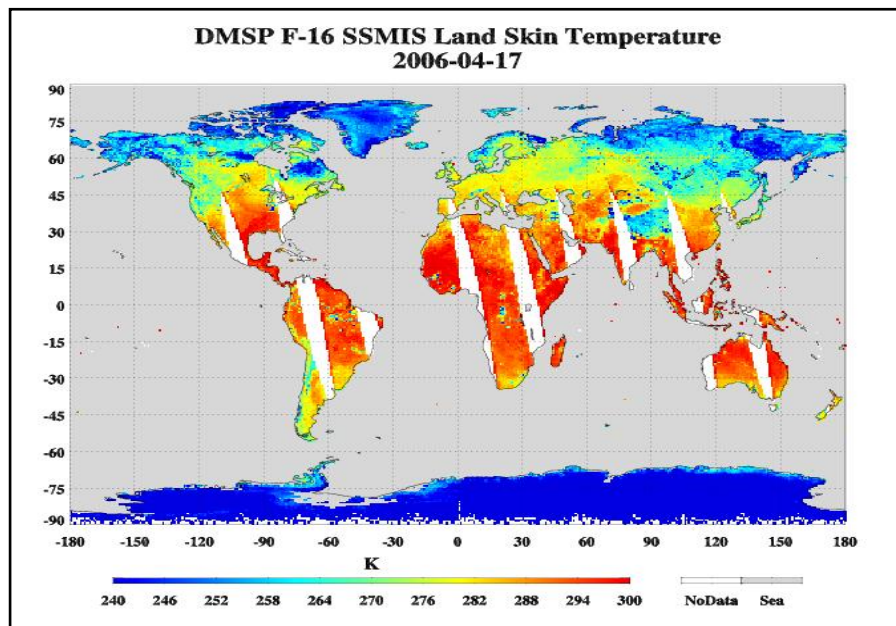


(b)

Figure 11 (a) Total Precipitable Water Retrieved from DMSP F-15 SSM/I Imaging Channels on April 17, 2005. (b) Same as Figure-7 but from DMSP F-16 SSMI/S Imaging Channels

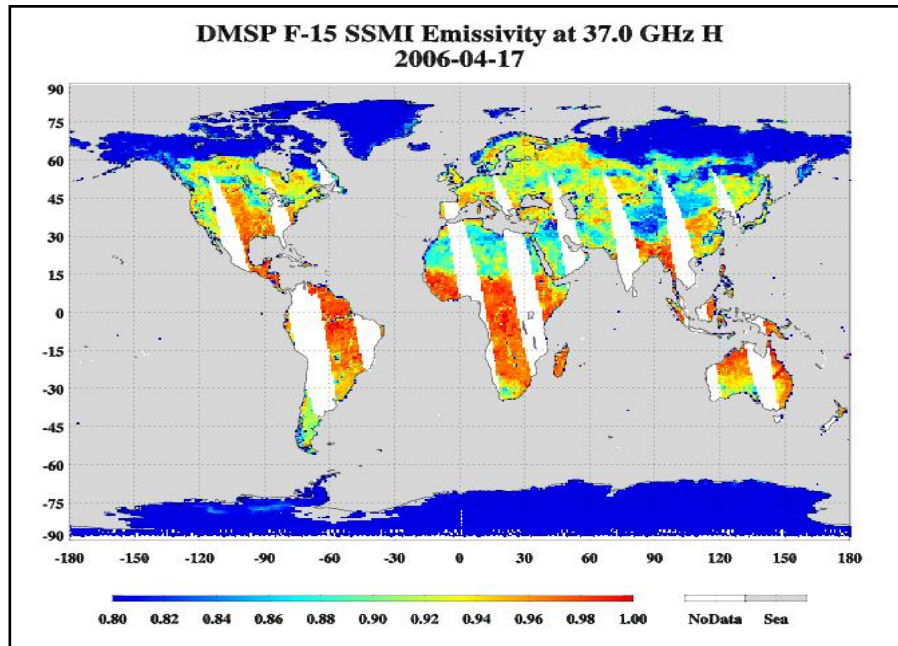


(a)

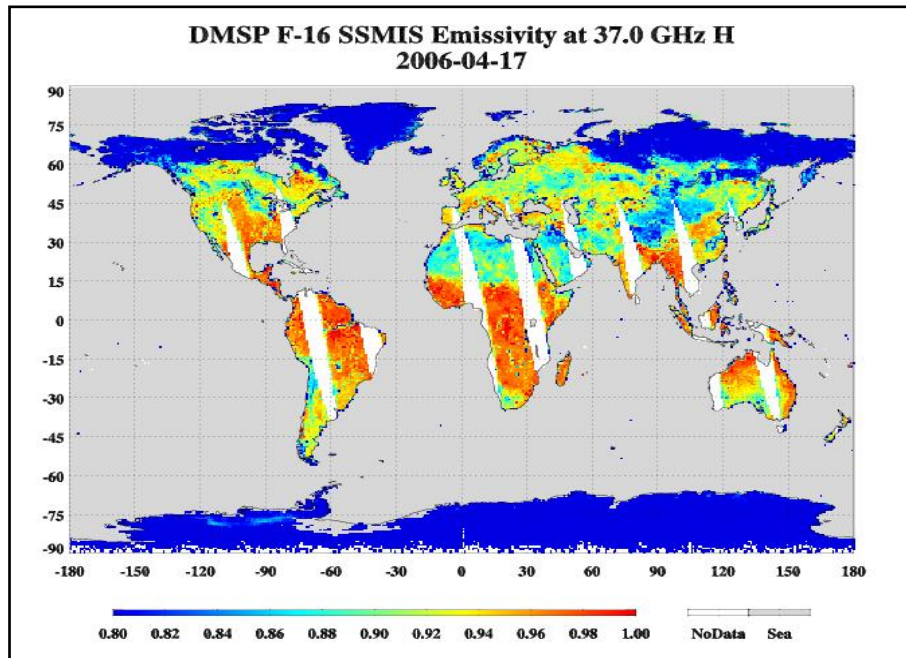


(b)

Figure12 (a) Land Surface Temperature Retrieved from DMSP F-15 SSM/I Imaging Channels on April 17, 2005. (b) Same as Figure-10 but from DMSP F-16 SSMI/S Imaging Channels.



(a)



(b)

Figure13 (a) Land Emissivity at 37.0 GHz Horizontal Polarization Retrieved from DMSP F-15 SSM/I Imaging Channels on April 17, 2005. (b) Same as Figure-13 but from DMSP F-16 SSMI/S Imaging Channels.

4 IMPACTS OF F16 SSMIS RECALIBRATION

Direct benefits from improved cal/val algorithms will be more satellite data used in NWP models and by forecasters, resulting in improved NWP analysis fields, forecast score, and climate trend reanalysis. A good example is the first Special Sensor Microwave Imager and Sounder (SSMIS) onboard DMSP F16 satellite. Currently, the NWP community has not learned on effective handling SSMIS sounding data because the measurements display some regional anomalies (see Fig. 2). STAR is working closely with Fleet Numerical Meteorological and Oceanography Center (FNMOOC) and NRL on developments of improved SSMIS calibration. Our beta version pf SSMIS calibration can now eliminate the antenna emission and solar contamination on calibration targets.

4.1 Performance of Recalibrated SSMIS Data

Figure 14 displays the SSMIS brightness temperature differences between observations and simulations at 54.4 GHz, where three types of SSMIS data are used, e.g., NRL TDR data, NESDIS CTDR data, UKMO CTDR data. Figures 15a and 15b are the histograms of SSMIS/AMSU brightness temperature differences and their standard deviations at channels 2 – 7 (Kazumori et al., 2007). It is found that the NESDIS SSMIS CTDR data at channels 2- 7 has a comparable quality to AMSU. With a set of quality control (QC) criteria, there are about 44% in channel 2 and 72% in channel 4 of the data used in the NCEP Girded Statistical Interpolation System (GSIS), as shown in Figure 16.

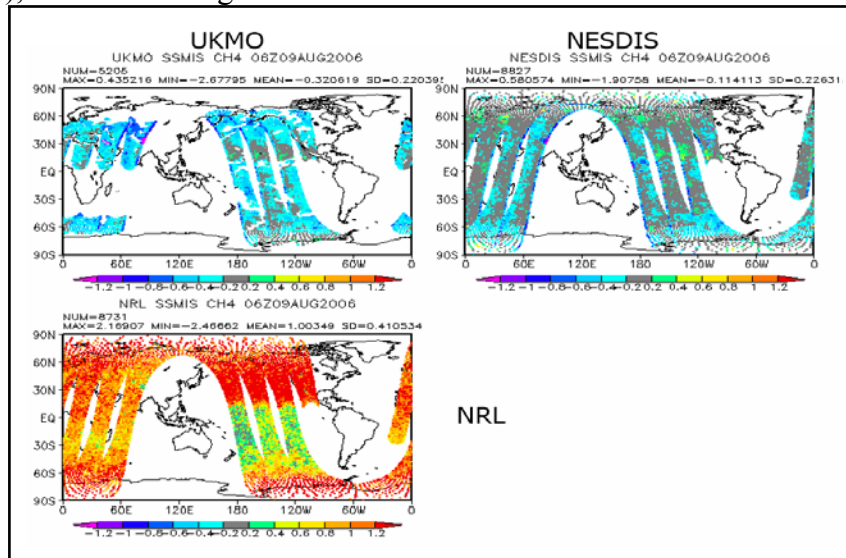
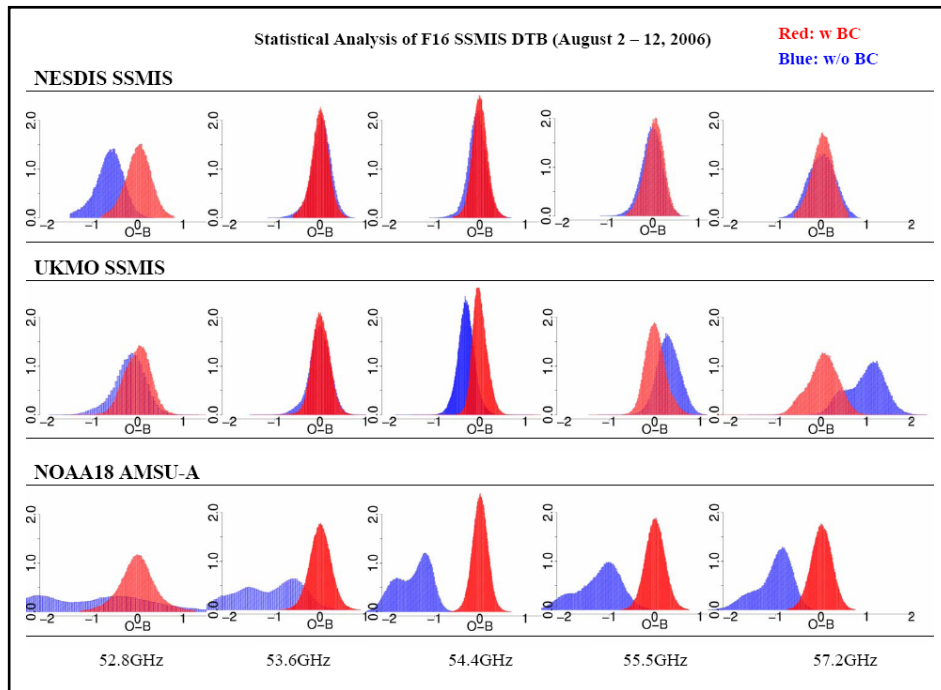
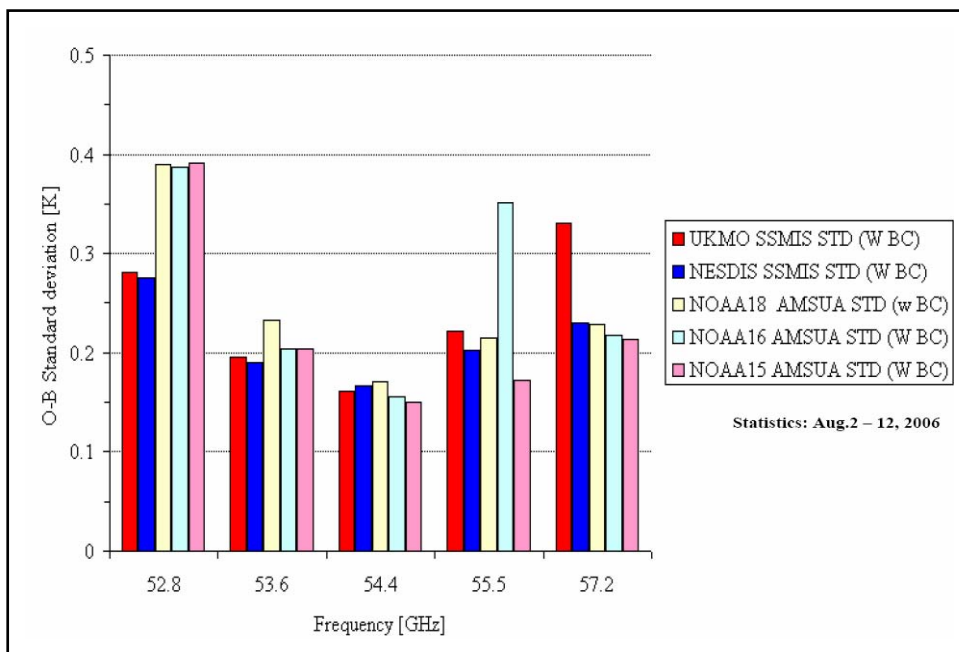


Figure 14 SSMIS brightness temperature differences at 54.4 GHz, where three types of SSMIS data are used, e.g., NRL TDR data, NESDIS CTDR data, UKMO CTDR data.



(a)



(b)

Figure 15 SSMIS brightness temperature differences (observations and simulations) and their standard deviations at 52.8, 53.6, 54.4, 55.5, 57.3 GHz, where three types of SSMIS data are used, e.g., NRL TDR data, NESDIS CTDR data, UKMO CTDR data (Kazumori et al., 2007).

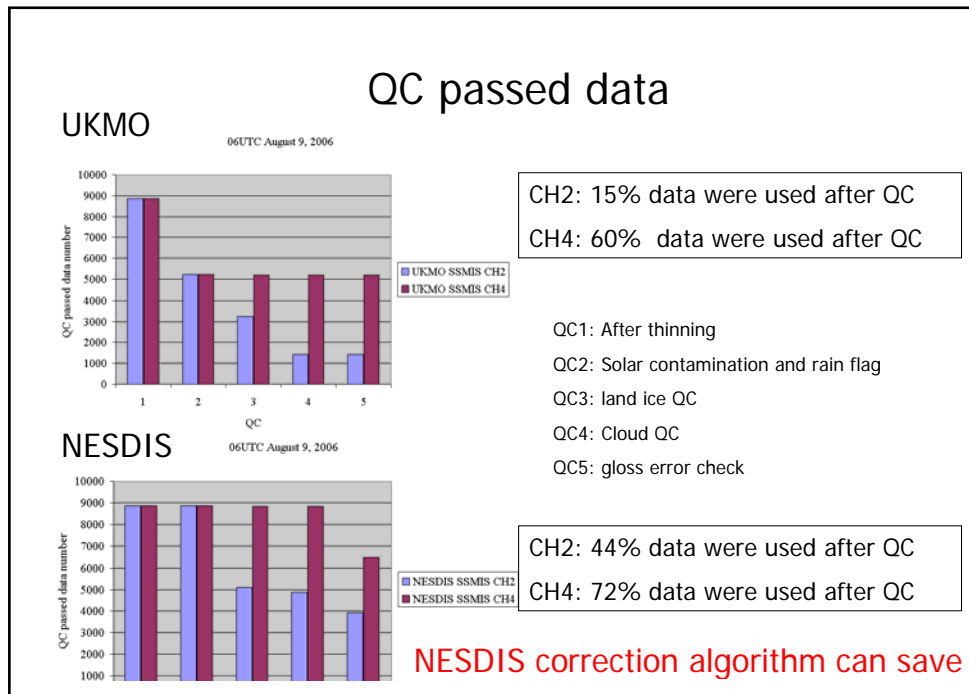


Figure 16 Number of SSMIS data used in the NCEP Girded Statistical Interpolation System after a certain quality control criteria, (Kazumori et al., 2007).

4.2 Impacts on NWP Analysis, Forecast and Climate Reanalysis

To demonstrate the impacts of NESDIS SSMIS CTDR data on NWP forecast weather model, STAR and EMC designed an assimilation experiment of SSMIS data from F16 for the period August 2 and October 7, 2006, through NCEP Gridded Statistical Interpolation System (Kazumori et al., 2007). Figure 17 displays the vertical distribution of RMS difference between the ‘Control’ and ‘Test’ results over global areas, where ‘Control’ is defined to be the forecast analysis only with AMSU data, ‘Test’ the forecast analysis with both AMSU and NESDIS (UK) SSMIS data. As the RMS difference is negative, the impact of the ‘Test’ data is positive. It is found that NESDIS SSMIS data produces positive impacts at most of heights over most of global areas. Especially, the great improvement is detected in the stratosphere.

Figures 18a and 18b show the anomaly correlation using the NESDIS and UK SSMIS data at 500 mb geopotential height over North Hemisphere (NH) and South Hemisphere (SH), respectively.

Figures 19a and 19b are the time series of the anomaly correlation at 500 mb geopotential height over both NH and SH from August 7 to October 7, 2006. The slightly positive impact is observed in both NESDIS and UK SSMIS data over NH and SH. Figure 20 displays the impact of NESDIS SSMIS data on vertical wind vector prediction by using NCEP global forecast model. It is seen that the NESDIS SSMIS data slightly improves the quality of vertical wind vector prediction. This further demonstrates the success of NESDIS SSMIS recalibration preprocessor for various LAS channels.

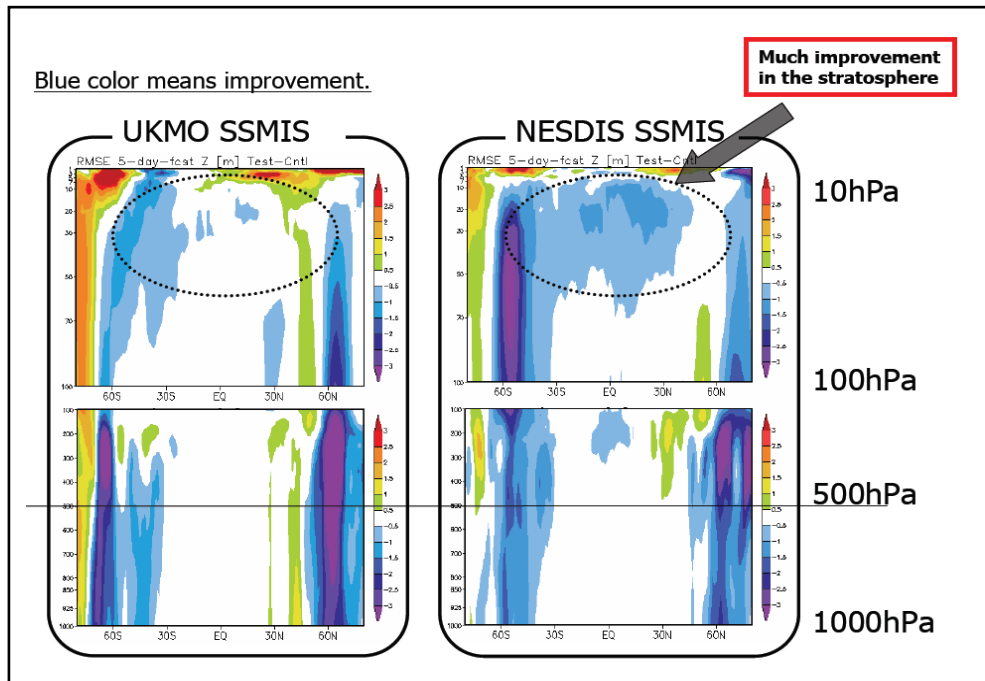
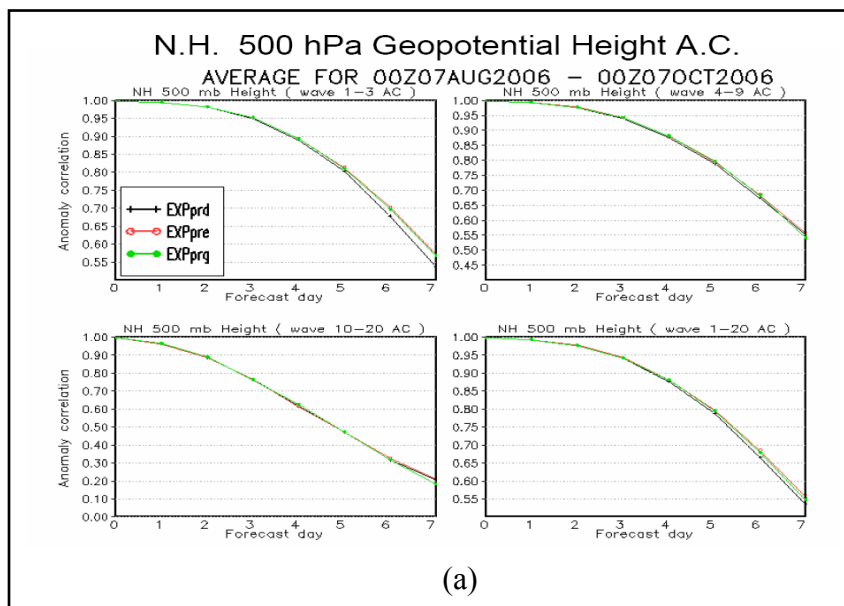


Figure 17 Vertical distribution of RMS difference between the ‘Control’ and ‘Test’ results over global areas, where ‘Control’ is defined to be the forecast analysis only with AMSU data, ‘Test’ the forecast analysis with both AMSU and NESDIS (UK) SSMIS data, (Kazumori et al., 2007).



(a)

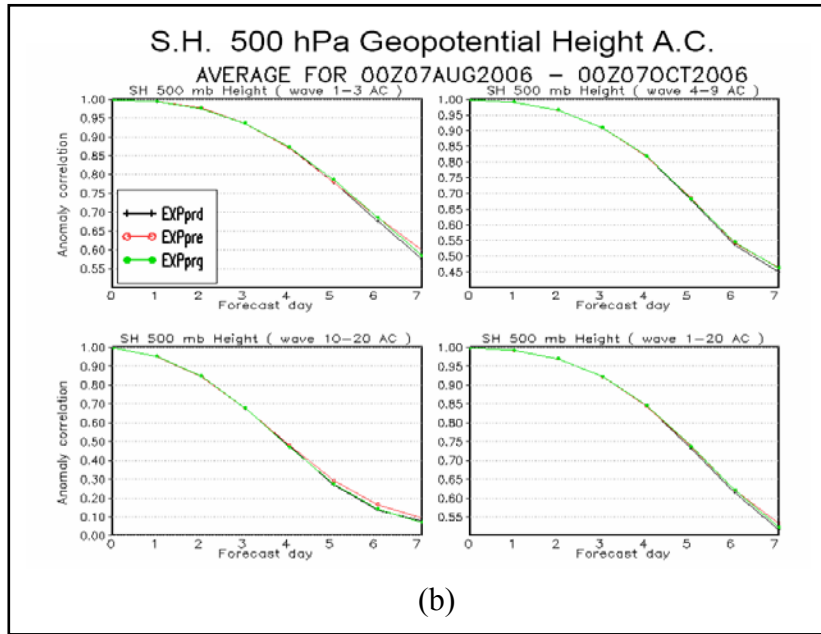
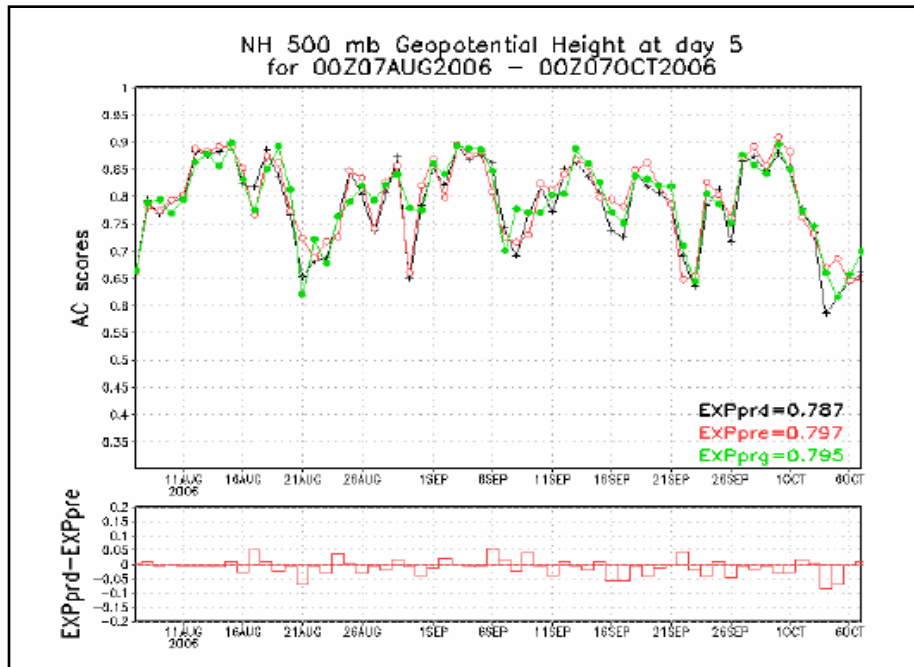
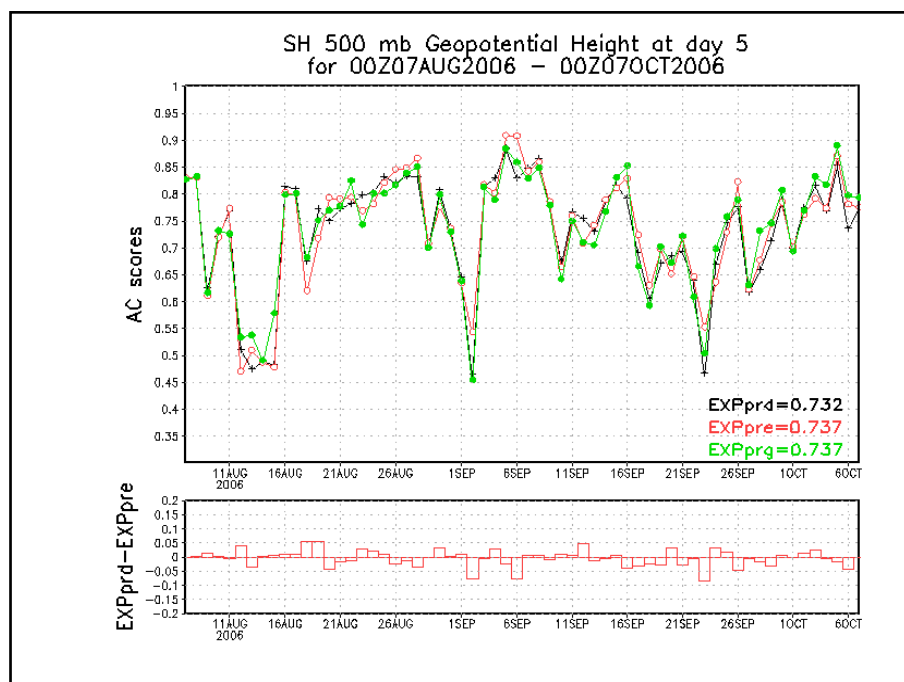


Figure 18 Anomaly correlation using the NESDIS and UK SSMIS data at 500 mb geopotential height over North Hemisphere (NH) in (a) and South Hemisphere (SH) in (b), (Kazumori et al., 2007).





(b)

Figure 19 Time series of anomaly correlation using the NESDIS and UK SSMIS data at 500 mb geopotential height over North Hemisphere (NH) in (a) and South Hemisphere (SH) in (b), (Kazumori et al., 2007).

Besides, using the Community Radiative Transfer Model (CRTM) (Weng et al., 2005), we can now assimilate radiance observations from cloudy and rainy areas. The new technique produces a temperature field in Hurricane Katrina that is more detailed, and that better resolves the warm core of the hurricane, as shown in Fig. 21 (Liu and Weng, 2006), where, the radiance observations are from the Special Sensor Microwave Imager and Sounder (SSMIS) instrument on the DMSP satellite. The new data assimilation technique improves the analysis of temperature fields (shown in the right panels) at two levels in Hurricane Katrina, compared with the same fields in the control run, in the left panels. The other tests that directly assimilate SSMIS upper stratospheric and mesospheric sounding channels also show reduced cold biases in NCEP global analysis system (Liu et al., 2007). The SSMIS brightness temperature can also reveal directly the hurricane warm core feature (Liu and Weng, 2006) and stratospheric temperature anomalies due to its constant viewing angle.

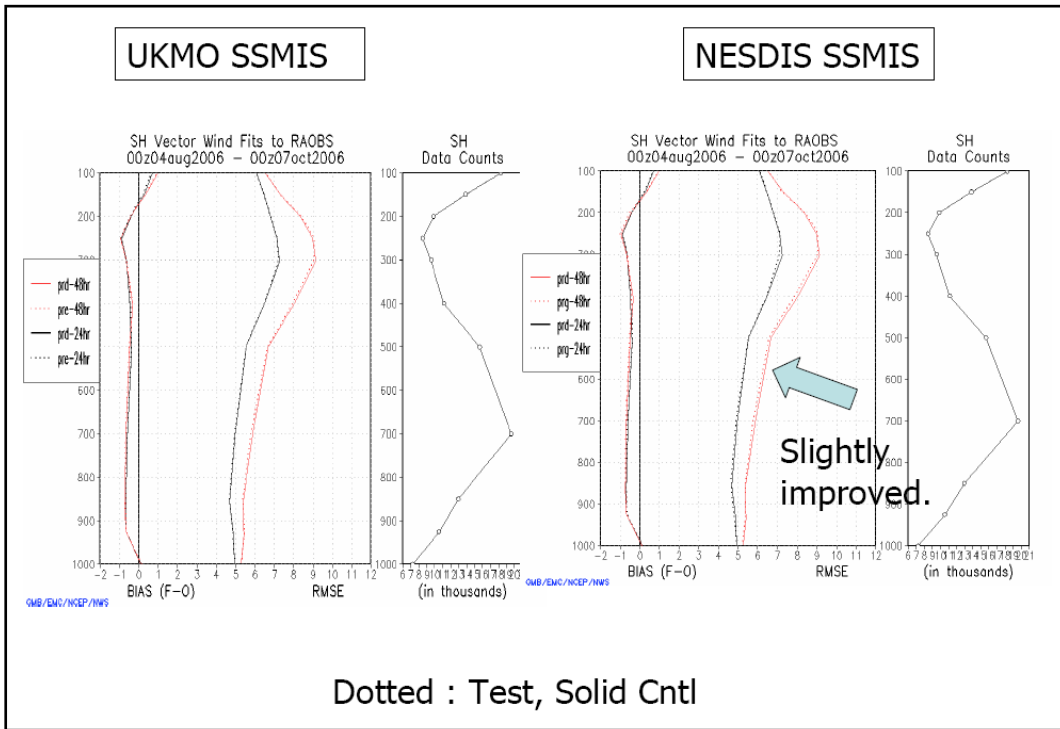


Figure 20 The bias and RMS distribution of vertical vector wind fit to RAOB (radiosonde data) in NCEP global forecast model analysis products, where either NESDIS SSMIS or UK SSMIS data is assimilated into NCEP global forecast model.

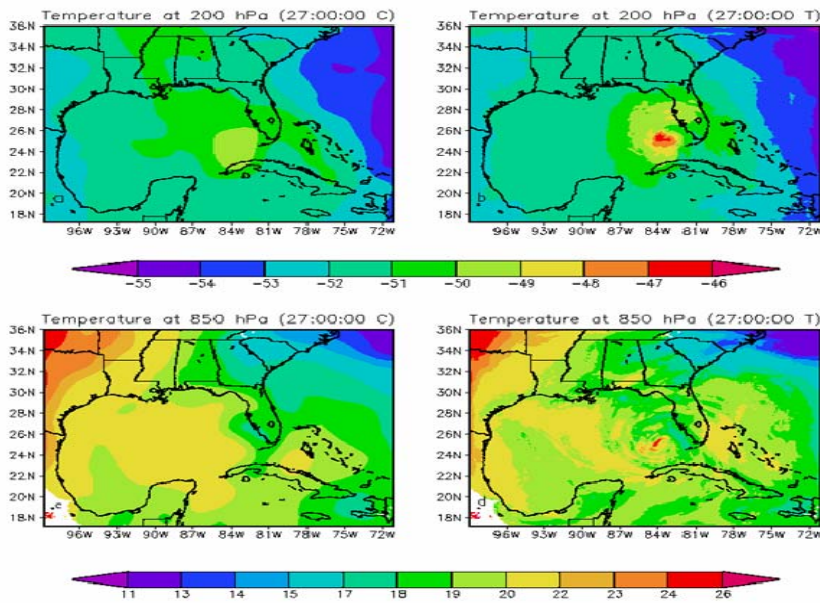


Figure 21 Temperature fields from NCEP global weather forecast model, where the radiance observations in the

right panels are from the Special Sensor Microwave Imager and Sounder (SSMIS) instrument on the DMSP satellite. The new data assimilation technique improves the analysis of temperature fields (shown in the right panels) at two levels in Hurricane Katrina, compared with the same fields in the control run, in the left panels.

5 STRENGTH AND WEAKNESS

5.1 NESDIS Calibration Strengths

As described above, NESDIS SSMIS recalibration preprocessor processes SSMIS TDR differently according to lower, upper, and imager channels. Among LAS channels, the antenna emission and the solar contamination on SSMIS calibration targets are suitably corrected. Thus, the SSMIS CTDR data at different subgroup channels demonstrates its unique quality. The NESDIS SSMIS preprocessor has following strengths.

Data Quality and Usage:

- (1) The solar radiation striking the surface of the warm load tines has been suitably corrected by primarily using the FFT analysis, so the SSMIS data with solar intrusion may be saved, which is 30 ~ 40 % of the data. This significantly increases the usage of SSMIS data in the satellite data assimilation system (Fig. 16).
- (2) The residual error in SSMIS observations at channels 3 – 7 is relatively small (Figs. 15 and 16). The good performance of those channels results in much improvements in stratosphere in NCEP global forecast model (Fig. 17), and results in a slightly improvement in vertical wind prediction (Fig. 20).
- (3) SSMIS imager channels (channels 12- 18) have been calibrated from the Simultaneous Conical Overpasses observations. With the remapping coefficients in Table 2, SSMIS observations at seven imager channels can be converted to F15 SSMI channels. Importantly, the nonlinear effect on those imager channels has been demonstrated to be important in future SSMI and SSMIS reprocessing.

Data Impact on Global Forecast Model:

An obviously positive impact is detected in the stratosphere; the impact is also positive or neural in the lower troposphere.

Data Integrity:

The temperatures in the TDR file have been modified in a manner that the original integrity of the data is preserved. The Fourier filtered gain corrections can be backed out for subsequent analysis. The reflector emission correction is applied downstream using the estimated reflector face temperature and the frequency dependent emissivity.

Robustness:

The IDL preprocessor has been running at FNMOC for over a year. It runs in about 6 seconds per rev on an older Sun blade processor.

5.2 NESDIS Calibration Weakness

- (1) Slightly large noise in Channel 2.
- (2) Upper channels are to be assessed.

References

- Bell, W., S. English, S. Swadley, 2005: SSMIS calibration issues, 1st *SSMIS Working Group Meeting*, Monterey, CA.
- Bell, W., 2006: A preprocessor for SSMIS radiances scientific description, http://www.metoffice.com/research/interproj/nwpsaf/ssmis_pp/, METOffice, UK.
- Bell, W., S. English, B. Candy, F. Hilton, N. Atkinson, N. Baker, S. Swadley, W. Campbell, N. Bormann, G. Kelly, M. Kazumori, 2007: The Assimilation of SSMIS Radiances in Numerical Weather Prediction Models', submitted to TGARS Special Issue on SSMIS.
- Boukabara, S., F. Weng, and Q. Liu, 2006: Passive microwave remote sensing of extreme weather events using NOAA-18 AMSUA and MHS, *IEEE Trans Geos Remote Sens.*, (revised)
- Cao, C., M. Weinreb, and H. Xu, 2004: Predicting simultaneous nadir overpasses among polar-orbiting meteorological satellites for the intersatellite calibration of radiometers, *J. Atmospheric and Oceanic Technology*, **21**, 537-542.
- Ferraro, R.R., F. Weng, N. Grody, and A. Basist, 1996: An eight year (1987-1994) time series of rainfall, clouds, water vapor, snow and sea ice derived from SSM/I measurements, *Bull. Amer. Meteor. Soc.*, **77**, 891-905.
- Ferraro, R.R., 1997: SSM/I derived global rainfall estimates for climatological applications. *J. Geophys. Res.*, **102**, 16,715-16,735.
- Iacovazzi, R. A., and C. Cao, 2007: Reducing uncertainties of SNO-estimated AMSU-A relative calibration biases at surface-influenced channels, to be submitted to *J. Atmospheric and Oceanic Technology*.
- Kazumori, M., B. Yan, F. Weng, J. Derber, 2007: Impact study of DMSP F-16 SSMIS radiances in NCEP global data assimilation system, to be submitted.
- Kondragunta, S., L. E. Flynn, A. Neuendorffer, A. J. Miller, C. Long, R. Nagatani, S. Zhou, T. Beck, E. Beach, R. McPeters, R. Stolarski, P. K. Bhartia, M. T. DeLand, L. -K. Huang, Vertical structure of the anomalous 2002 Antarctic ozone hole, *J. of Atmos. Sci.*
- Liu, Q. and F. Weng, 2006a: Detecting Warm Core of Hurricane from the Special Sensor Microwave Imager Sounder, *Geophys. Res. Letters*, **33**, 2006
- Liu, Q., and F. Weng, 2006b: Radiance Assimilation in Studying Hurricane Katrina, *Geophysical Research Letters*, **33**, doi:10.1029/2006GL027543
- Poe, G., K. Germain, J. Bobak, S. Swadley, J. Wessel, B. Thomas, J. Wang, B. Burns, 2001, DMSP Calibration/Validation Plan for the Special Sensor Microwave Imager Sounder (SSMIS).

- Sun, N. and Weng, F., 2007: Evaluation of SSMIS environment data records, submitted to *TGARS Special Issue on the DMSP SSMIS*.
- Swadley, S., G. Poe, A. Uliana, D. Kunkee, 2005: SSMIS Cal/Val calibration anomaly analysis, NOAA-JCSDA seminar, Washington DC
- Weng, F., N. Grody, R. Ferraro, Q. Zhao, and C. Chen, Global Cloud Water Distribution Derived from Special Sensor Microwave Imager/Sounder and its Comparison with GCM Simulation, *Adv. Space Res.*, Vol. 19, No. 3, 1997, pp. 407-411.
- Weng, F., B. Yan, N. Sun, 2005: Correction of SSMIS radiance anomalies, 1st SSMIS Working Group Meeting, Monterey, CA.
- Weng, F., 2006, Advances in radiative transfer modeling in support of satellite data assimilation, *J. Atmos. Sci.* (Submitted)
- Weng, F., B. Yan, Q. Liu, S. Boukabara, H. Yong, N. Sun, and R. Ferraro, 2007: Initial Demonstration of Special Sensor Microwave Imager and Sounder (SSMIS) Products and Their Applications in Weather and Climate Analyses , submitted to *Bulletin of American Meteorological Society*
- Yan B. and F. Weng, 2002: A fifteen-year (1987-2002) climatology of microwave land emissivity, Proceedings of SPIE for Microwave Remote Sensing of the Atmosphere and Environment, Hangzhou, China.
- Yan, B., F. Weng, and K. Okamoto, 2004: Improved Estimation of Snow Emissivity from 5 to 200 GHz, 8th Specialist Meeting on Microwave Radiometry and Remote Sensor Applications, Rome, Italy.
- Yan, B. and F. Weng, 2007a: Recalibration of Special Sensor Microwave Imager and Sounder (SSMIS) for Lower Atmospheric Sounding Channels, to be submitted to *Journal of Atmospheric and Oceanic Technology*.
- Yan, B. and F. Weng, 2007b: Intercalibration between Special Sensor Microwave Imager and Sounder (SSMIS) and Special Sensor Microwave Imager (SSM/I), submitted to *TGARS Special Issue on the DMSP SSMIS*.
- Zou, C., M. D. Goldberg, Z. Cheng, N. C. Grody, J. T. Sullivan, C. Cao, and D. Tarpley (2006), Recalibration of microwave sounding unit for climate studies using simultaneous nadir overpasses, *J. Geophys. Res.*, **111**, doi:10.1029/2005JD006798.